Cellular/Molecular

A Ca²⁺ Threshold for Induction of Spike-Timing-Dependent Depression in the Mouse Striatum

Tomomi Shindou, Mayumi Ochi-Shindou, and Jeffery R. Wickens

Okinawa Institute of Science and Technology, Okinawa 904-0412, Japan

The striatum is the principal input nucleus of the basal ganglia, receiving glutamatergic afferents from the cerebral cortex. There is much interest in mechanisms of synaptic plasticity in the corticostriatal synapses. We used two-photon microscopy and whole-cell recording to measure changes in intracellular calcium concentration ($[Ca^{2+}]_i$) associated with spike-time-dependent plasticity in mouse striatum. Uncaging glutamate adjacent to a dendritic spine caused a postsynaptic potential at the soma and a rise in spine $[Ca^{2+}]_i$. Action potentials elicited at the soma raised both dendrite and spine $[Ca^{2+}]_i$. Pairing protocols in which glutamate uncaging preceded action potentials by 10 ms (pre-post protocol) produced supralinear increases in spine $[Ca^{2+}]_i$ compared with the sum of increases seen with uncaging and action potentials alone, or timing protocols in which the uncaging followed the action potentials (post-pre protocols). The supralinear component of the increases in $[Ca^{2+}]_i$ were eliminated by the voltage-sensitive calcium channel blocker nimodipine. In the adjacent parent dendrites, the increases in $[Ca^{2+}]_i$ were neither supralinear nor sensitive to the relative pre-post timing. In parallel experiments, we investigated the effects of these pairing protocols on spike-timing-dependent synaptic plasticity. Long-term depression (t-LTD) of corticostriatal inputs was induced by pre-post but not post-pre protocols. Intracellular calcium chelators and calcium antagonists blocked pre-post t-LTD, confirming that elevated calcium entering via voltage-sensitive calcium channels is necessary for t-LTD. These findings confirm a spine $[Ca^{2+}]_i$ threshold for induction of t-LTD in the corticostriatal pathway, mediated by the supralinear increase in $[Ca^{2+}]_i$ associated with pre-post induction protocols.

Introduction

Striatal spiny projection neurons receive corticostriatal synapses on their dendritic spines (Wilson, 1986). These synapses are glutamatergic and produce EPSPs mediated by activation of AMPA and NMDA receptors (Herrling et al., 1983; Calabresi et al., 1996; Kita, 1996). Because the striatum is involved in certain types of learning (Packard and Knowlton, 2002; Yin and Knowlton, 2006), activity-dependent plasticity in the corticostriatal synapses has been extensively studied (Calabresi et al., 2007; Surmeier et al., 2007; Wickens, 2009). High-frequency stimulation causes long-term depression (LTD) (Calabresi et al., 1992, 1994; Walsh, 1993; Wickens et al., 1996; Kerr and Wickens, 2001; Bonsi et al., 2003), which requires activation of voltage-sensitive calcium channels (VSCCs) and an increase in intracellular calcium ions ($[Ca^{2+}]_i$) postsynaptically (Calabresi et al., 1992, 1994; Bonsi et al., 2003; Adermark and Lovinger, 2007).

Corticostriatal neurons naturally fire at low rates (Bauswein et al., 1989; Turner and DeLong, 2000). Under such sparse firing conditions, high-frequency firing does not occur, so the physiological relevance of LTD can be questioned. It has been shown, however, that single presynaptic spikes can modify $[Ca^{2+}]_i$ in

spiny projection neurons. However, there are strict timing requirements. In cell cultures, Kerr and Plenz (2004) found that $[Ca^{2+}]_i$ was maximal when synaptic inputs occurred within 10–20 ms of the onset of spontaneous depolarizations, due to back-propagating action potentials (bAPs) from the soma (Kerr and Plenz, 2002, 2004). The time dependence required NMDA receptors (Kerr and Plenz, 2004). Similarly, Carter and Sabatini (2004) found that pairing of bAPs with glutamate uncaging generated additional $[Ca^{2+}]_i$ in dendritic spines due to enhanced Ca^{2+} influx through NMDA receptors.

Even under sparse activity conditions, the increased $[Ca^{2+}]_i$ caused by pairing has the potential to engage spike-timing-dependent plasticity (STDP) mechanisms, as has been shown in other systems. In the striatum, however, the results obtained to date seem contradictory. Fino et al. (2005) reported that spike-time-dependent LTD (t-LTD) was induced when presynaptic spikes preceded postsynaptic spikes (pre-post timing), and reversed timing (post-pre timing) produced long-term potentiation (t-LTP). In contrast, Pawlak and Kerr (2008) found that pre-post timing caused t-LTP and reverse timing caused t-LTD. Shen et al. (2008) found that pre-post protocols produced t-LTP in dopamine D1 receptor-expressing cells, but under dopamine-depleted conditions, D1 cells showed LTD. In contrast, D2 cells, which showed LTD in response to post-pre protocols, exhibited LTP under dopamine-depleted conditions. Together, the findings suggest that spike-time-dependent plasticity occurs in the corticostriatal synapses, but the precise time dependence may vary according to experimental conditions.

The present experiments investigated the relationship between dendritic spine $[Ca^{2+}]_i$ transients and STDP using two-

photon imaging. We found that pre-post protocols caused larger spine $[Ca^{2+}]_i$ transients than post-pre protocols. Pre-post protocols induced t-LTD, which was Ca^{2+} dependent. We suggest there is a threshold spine $[Ca^{2+}]_i$ level for induction of t-LTD, which is exceeded during pre-post protocols as a result of nonlinear interaction of bAPs with synaptic input in dendritic spines.

Materials and Methods

Animals were handled in accordance with protocols approved by the Okinawa Institute of Science and Technology Animal Care and Use Committee. The experiments were performed on male C57BL/6 mice (age, 2–4 months). Animals were deeply anesthetized with sodium pentobarbital (80 mg/kg; Wako) and then perfused transcardially for 2 min with cold-modified artificial CSF (ACSF) containing the following (in mM): 50.0 NaCl, 2.5 KCl, 7.0 $MgCl_2$, 0.5 $CaCl_2$, 1.25 NaH_2PO_4, 25.0 $NaHCO_3$, 95.0 sucrose, and 25.0 glucose and saturated with 95% O_2/5% CO_2. The brain was removed quickly and chilled. Slices (300 μm thick) containing the striatum were cut on a VT1000S microtome (Leica) in an oblique plane, 45° rostal-up to the horizontal (Shindou et al., 2008). Slices were then incubated in oxygenated standard ACSF maintained at a temperature of 36°C for 1 h. The standard ACSF had the following composition (mM): 120.0 NaCl, 2.5 KCl, 2.0 $CaCl_2$, 1.0 $MgCl_2$, 25.0 $NaHCO_3$, 1.25 $NaHPO_4$, 15.0 glucose. After incubation, a single slice was transferred to a recording chamber placed on the stage of an upright microscope and perfused (3–4 ml/min) with oxygenated ACSF at 30°C. The remaining slices were kept in a holding chamber containing oxygenated ACSF at room temperature until required.

Electrophysiology. Whole-cell recordings from spiny projection neurons in dorsomedial striatum were obtained with infrared differential interference contrast microscopy. A Molecular Devices Multiclamp 700B amplifier was used to provide current-clamp capability and to record glutamatergic EPSPs. Patch pipettes (2–4 MΩ) were filled with internal solution containing the following (in mM): 115.0 K gluconate, 1.2 $MgCl_2$, 10.0 HEPES, 4.0 ATP, 0.3 GTP, and 0.5% biocytin; pH 7.2–7.4.

Calcium imaging. Two-photon imaging of dendritic spines was performed with an upright microscope (FV1000MPE; Olympus) equipped with a 60× objective (numerical aperture, 0.9; Olympus). Striatal spiny neurons were filled via the recording pipette with a combination of the Ca^{2+}-insensitive dye Alexa 594 (30 μM; Invitrogen) and Ca^{2+}-indicator Fluo-5F (300 μM, K_D 2.3 μM; Invitrogen) for 10–20 min before imaging. Fluo-5F and Alexa 594 were excited using 850 nm light to monitor calcium signals and spine morphology, respectively, and fluorescence emission was acquired at 400–570 nm (green) and 590–650 nm (red) for Fluo-5F and Alexa 594, respectively. Responsive spines on dendrites 30–60 μm (average 47 μm) from the soma were identified using frame scans. For quantitative measurements, line scans (500 Hz) were used. Changes in Ca^{2+} levels were based on the ratio of green fluorescence relative to baseline red fluorescence (R). We performed *in situ* calibration of R by whole-cell perfusion with internal solutions containing 10 mM EGTA or 10 mM Ca^{2+}, which provided estimates of R_{min} and R_{max} as 0.203 and 2.013, respectively. Ca^{2+} changes in fluorescence are expressed as the following: $[Ca^{2+}] = K_D(R - R_{min})/(R_{max} - R)$ (Yasuda et al., 2004; Noguchi et al., 2005). Given that R before stimulation (R_0) was similar to R_{min}, we used the relation $\Delta R = R - R_0$ to estimate $[Ca^{2+}]_i$; therefore, we expressed $[Ca^{2+}]_i$ as $K_D\Delta R/(R_{max} - R_{min} - \Delta R)$ (Noguchi et al., 2005). R_0 was the averaged fluorescence over 50 ms immediately before stimulation. Dual exponential fits to the fluorescence transients yielded the peak amplitude and the rising and decay phase time constants. Fluorescence traces are averages of three to five trials. Each spine measured was from a different cell and all protocols were applied to each spine, permitting within-subject comparisons. Two-photon excitation at 720 nm (0.5 ms pulse) was used to cause photolysis of MNI-caged L-glutamate (Tocris Bioscience). MNI-glutamate (20 mM) was applied via a micropipette positioned above slice.

Plasticity experiments were conducted separately on slices prepared using identical procedures. EPSPs were elicited in spiny neurons by extracellular stimulation with bipolar electrodes placed in the corpus callosum. Stimulation intensity (0.01–0.5 mA, 200 μs duration) was
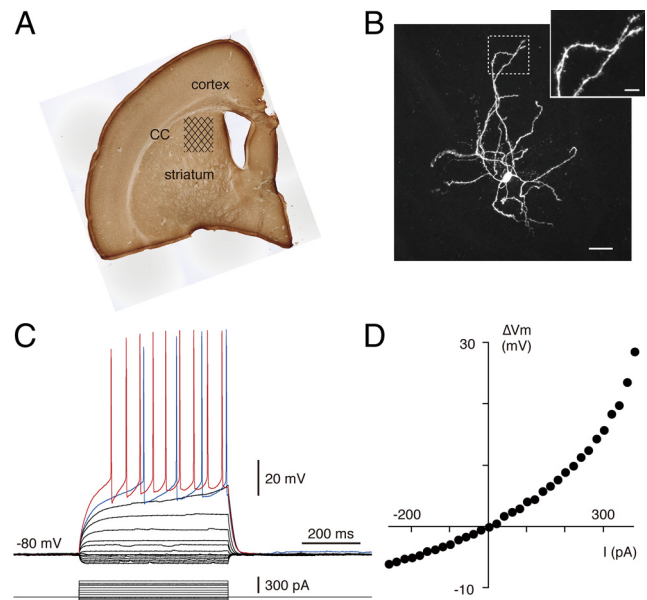

Figure 1. Electrophysiological characterization of striatal spiny neurons. *A*, Photograph of the parahorizontal corticostriatal slice preparation, showing the position of the cortex, striatum, and corpus callosum (CC). The cells in the study were in the hatched region. *B*, Micrograph of a neuron injected with biocytin after recording in the whole-cell configuration, showing typical morphological features of spiny projection neurons (scale bar, 20 μm). Inset shows spiny distal dendrites (scale bar, 5 μm). *C*, Voltage responses to hyperpolarizing and depolarizing current pulses showing the characteristic responses of spiny projection neurons. *D*, Current (I) versus voltage (Vm) relation showing inward rectification typical of spiny projection neurons.

adjusted to evoke baseline single-component EPSPs with amplitudes of 1–5 mV. Baseline EPSPs were recorded for 10 min at 0.05 Hz stimulation rate. During pairing, EPSPs were evoked together with one or three action potentials (APs) elicited by current injection at 0.1 Hz, 60 times. For STDP experiments using caged glutamate, photolysis of MNI-glutamate using a UV flash lamp system (JML-C2; Rapp Opto Electronic) during the pairing condition replaced electrical stimulation of the cortex. In these experiments, MNI-glutamate (1–10 mM) was applied via a micropipette positioned above the slice and uncaging parameters were adjusted to produce an uncaging-evoked EPSP (uEPSP) with amplitude matching the baseline EPSPs of 1–5 mV. A time interval Δt was defined as the time between the peak of the first AP and the onset of the EPSP. The change in EPSP amplitude was evaluated by averaging responses over an interval 10–20 min after the end of the pairing period. For group averages, responses were expressed as percentage change from the baseline EPSP amplitude. Data are presented as mean ± SEM.

After recording was completed, slices containing biocytin-loaded cells were fixed by immersion in 4% paraformaldehyde in 0.1 M phosphate buffer (PB) overnight at 4°C. They were rinsed in PB for 30 min, and then incubated in 15% and 30% sucrose for 30 min and 1 h, respectively. The slices were reacted with streptavidin-conjugated Alexa 488 (1:1000) in PB containing 0.4% Triton X for 2 h at room temperature, and mounted on slides.

Results

Whole-cell *in vitro* recordings were obtained from neurons located in dorsomedial striatum (Fig. 1A). Neurons were identified by staining of intracellularly injected biocytin or Alexa 594, and displayed medium-sized (10–15 μm diameter) somata, with several smooth primary dendritic branches and spine-encrusted secondary and tertiary dendrites (Fig. 1B). These neurons exhibited characteristic electrophysiological properties, including delay in action potential firing and onset of firing at low rates in response to depolarizing current pulses (Fig. 1C) and inward rectification (Fig. 1D). These properties collectively confirm the identity of
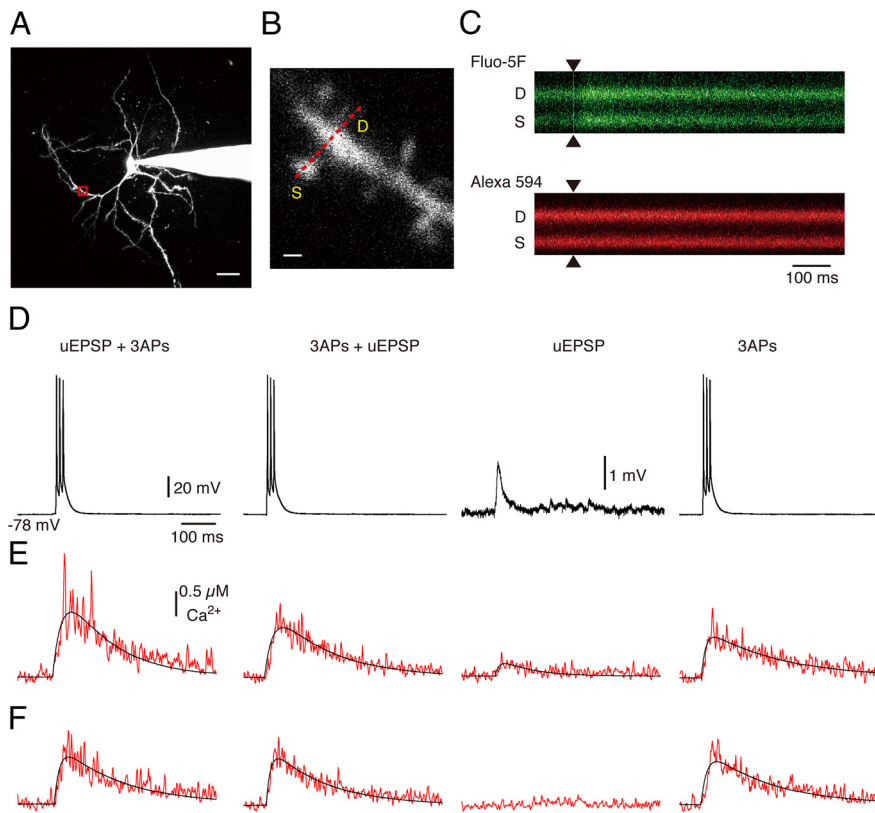
Figure 2. Comparison of $[Ca^{2+}]_i$ transients induced in dendrites and dendritic spines by different protocols. ***A***, Two-photon image of a spiny neuron, including the recording pipette attached at the soma. ***B***, Higher-power view of the region indicated by the red box in ***A***, showing dendritic spines (S) and adjacent dendrite (D). The dashed line indicates the direction of a line scan taken through the spine and dendrite. Scale bars: ***A***, 20 μm; ***B***, 1 μm. ***C***, An example line scan image for the Ca^{2+}-sensitive indicator Fluo-5F (green, top) and the Ca^{2+}-insensitive indicator Alexa Fluor 488 (red, bottom) showing the response to uncaging of MNI-glutamate followed by three APs at $\Delta t = 10$ ms (pre-post protocol). ***D***, Left to right, Somatic voltage recordings for a uEPSP and three APs at $\Delta t = 10$ ms (pre-post protocol), three APs and uEPSP at $\Delta t = -30$ ms (post-pre protocol), uEPSP alone, and three APs alone. ***E***, Dendritic spine $[Ca^{2+}]_i$ measurements corresponding to conditions in ***D***. ***F***, Dendritic $[Ca^{2+}]_i$ measurements corresponding to conditions in ***D***. Traces are averages of three successive responses. The equation $f(t) = Ca_{max}*(exp[-t/tau1] - exp[-t/tau2])/(tau1 - tau2)$ was used for curve fittings, where Ca_{max} is the peak concentration, tau1 is the time constant for the rising phase, and tau2 is the time constant for the falling phase of the calcium transient.

the neurons as spiny projection neurons (Wilson and Groves, 1980; Kawaguchi et al., 1989; Shindou et al., 2008). Two-photon microscopy observations were made on dendritic spines and adjacent dendritic shafts that were, on average, 46.8 μm distant from the soma. The observed spines were all on secondary dendrites, except for one spine on a tertiary dendrite.

Ca^{2+} transients in spines of spiny neurons

Synaptic activity may lead to activation of various sources of calcium influx into dendrites and dendritic spines, including influx through AMPARs (Carter and Sabatini, 2004) or by relief of the Mg^{2+} block of NMDARs by depolarization. To detect such influx, transient increases in $[Ca^{2+}]_i$ in the dendritic spine and dendritic shaft were measured using two-photon excitation fluorescence microscopy. Simultaneous two-photon uncaging of MNI-glutamate (20 mM) was to simulate the effects of a presynaptic spike (Fig. 2A–C) (Carter and Sabatini, 2004; Higley and Sabatini, 2008). uEPSPs were recorded simultaneously using patch electrodes in the whole-cell configuration (Fig. 2D). The intensity of two-photon excitation (0.5 ms pulses) was adjusted to elicit uEPSPs of similar amplitude to electrically evoked EPSPs obtained by low-intensity electrical stimulation in a set of plasticity experiments conducted in parallel and reported later in this

paper. We found that in response to glutamate uncaging, small $[Ca^{2+}]_i$ transients were induced in the spine head (0.23 ± 0.03 μM, $n = 11$; Fig. 2E). Smaller calcium transients were also measured in the dendritic shaft at the base of the activated spine (0.04 ± 0.02 μM, $n = 11$; Fig. 2F). The dendritic shaft peak concentration was substantially lower than the spine head, suggesting that the glutamate-evoked influx of calcium was mainly into the spine head.

bAPs from the soma may also give rise to calcium entry by activation of VSCCs, which have been localized in the spine head (Day et al., 2006). When action potentials were elicited by current pulses applied at the soma, $[Ca^{2+}]_i$ transients were induced in the spines (0.70 ± 0.11 μM, $n = 11$; Fig. 2E). Such transients were only observed when groups of three action potentials were evoked and were not seen in response to single somatic action potentials. Transients of similar peak concentration were measured in the adjacent dendritic shafts (0.80 ± 0.14 μM, $n = 11$; Fig. 2F). The similarity in amplitude of the spine head and dendritic shaft transients in response to action potential firing (in contrast to the different peak concentrations seen with glutamate uncaging) suggests activation of VSCC in both dendritic spine and dendritic shaft by the invasion of the bAPs.

Under pairing conditions, peak dendritic calcium levels have been reported to vary according to the precise timing of the bAPs in relation to synaptic inputs (Kerr and Plenz, 2002, 2004). In pairing experiments, uEPSPs and somatic action potentials were evoked in close temporal relation. When three action potentials were evoked after the uEPSP ($\Delta t = +10$ ms, pre-post stimulation), the pairing produced a large $[Ca^{2+}]_i$ transient (1.38 ± 0.15 μM, $n = 11$; Fig. 2E). Delaying the uEPSPs until after the action potentials ($\Delta t = -30$ ms, post-pre stimulation) resulted in a smaller $[Ca^{2+}]_i$ transient (0.92 ± 0.10 μM, $n = 11$; Fig. 2F). The pre-post transient was, on average, 50.0% greater than the post-pre transient.

The higher pre-post transients reflected nonlinear interaction of uEPSP and bAPs. Compared with the algebraic sum of the uEPSP and action potential responses, pre-post pairing produced a greater (150.5%) increase in spine $[Ca^{2+}]_i$. However, post-pre pairing resulted in a transient approximately equal to the linear sum of the uEPSP and action potentials responses (99.3%). This shows that pre-post protocols evoke supralinear increases in spine $[Ca^{2+}]_i$, in contrast to post-pre protocols.

In contrast to the nonlinear increase in calcium influx seen in dendritic spines with pre-post pairing, dendritic shaft $[Ca^{2+}]_i$ transients showed no difference between pre-post (0.96 ± 0.14 μM) and post-pre (0.98 ± 0.17 μM) conditions (Table 1). This suggests that dendritic shaft $[Ca^{2+}]_i$ transients are not sensitive to precise timing relationships in the same way as dendritic spine $[Ca^{2+}]_i$ transients.

Table 1. Effect of condition and location on peak and timecourse of $[Ca^{2+}]_i$

Condition	Spine peak Ca^{2+}	Shaft peak Ca^{2+}	Spine tau 1	Spine tau 2
uEPSP + 3 APs (pre-post, $n = 11$)	1.38 ± 0.15	0.96 ± 0.14	18.4 ± 3.8	191.0 ± 22.9
3 APs + uEPSP (post-pre, $n = 11$)	0.92 ± 0.10	0.98 ± 0.17	n.d.	n.d.
uEPSP + 1 AP (pre-post, $n = 4$)	0.33 ± 0.06	0.31 ± 0.02	28.3 ± 8.7	131.6 ± 42.4
1 AP + uEPSP (post-pre, $n = 4$)	0.33 ± 0.06	0.32 ± 0.01	n.d.	n.d.

n.d., Not determined.

We found that the number of action potentials evoked in pairing experiments is an important determinant of the sensitivity of peak $[Ca^{2+}]_i$ to relative timing of presynaptic and postsynaptic activity. When only one action potential was evoked after the uEPSP ($\Delta t = +10$ ms, pre-post stimulation), the $[Ca^{2+}]_i$ transient had a lower peak concentration than with three action potentials (0.33 ± 0.06 μM, $n = 4$) and was not significantly different from that seen when the uEPSPs were delayed until after the action potentials ($\Delta t = -10$ ms, post-pre stimulation; 0.33 ± 0.06 μM, $n = 4$). Using a single action potential in pre-post pairing produced only a 79.4% increase in spine $[Ca^{2+}]_i$ compared with the algebraic sum of the uEPSP and action potential responses; similarly, with post-pre pairing, the transient was only 80.7% of the linear sum of the uEPSP and action potentials (spine $[Ca^{2+}]_i$ uEPSP: 0.21 ± 0.03 μM, 1 AP: 0.20 ± 0.01 μM, $n = 4$). These data show that when only a single action potential is involved in pairing, there is no difference between pre-post and post-pre pairing protocols, and no evidence of supralinear $[Ca^{2+}]_i$ responses.

In summary, two-photon imaging data show that spine $[Ca^{2+}]_i$ is increased more by pre-post than post-pre spike timing. Moreover, the increase in the case of pre-post timing is supralinear, permitting the spine $[Ca^{2+}]_i$ to differentially signal a pre-post coincidence of activity. This differential signal was not seen in measurements of $[Ca^{2+}]_i$ from the dendritic shaft at the base of the spine. When only one action potential was evoked during pairing, dendritic spine $[Ca^{2+}]_i$ did not discriminate between pre-post and post-pre timing. These findings led to the question whether such $[Ca^{2+}]_i$ transients cause plastic changes in the associated synapses.

Pre-post timing induces spike-time-dependent LTD

To investigate the effects on long-term changes in synaptic efficacy of the same relative timing of presynaptic and postsynaptic activity as investigated in the imaging study, we first tested whether the uEPSP-spike pairing induced STDP. Since LTD is often expressed presynaptically, we used a bipolar electrical stimulating electrode placed in the corpus callosum to evoke test EPSPs, and used uncaging conditions that gave a uEPSP <5 mV, similar in amplitude to the test EPSP. As shown in Figure 3, this pairing protocol resulting in significant depression ($-20.4 \pm 3.1\%$, $n = 6$, $p < 0.01$).

For more detailed analysis of STDP, we conducted a separate set of experiments in which a bipolar electrical stimulating electrode was placed in the corpus callosum to evoke EPSPs. Electrical stimulus intensity was adjusted to give a subthreshold EPSP similar to the uEPSPs evoked by glutamate uncaging (1–5 mV amplitude). This low-intensity stimulus was used to avoid stimulating fine unmyelinated axons of the nigrostriatal dopaminer-
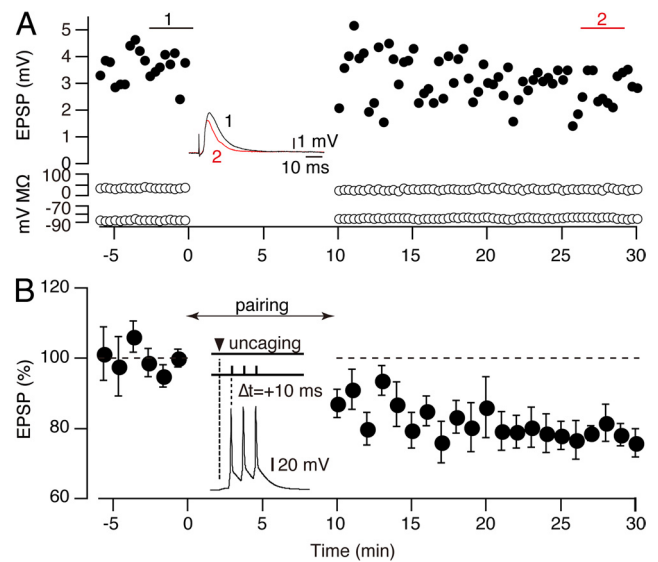

Figure 3. Spike-timing-dependent t-LTD induced by glutamate uncaging paired with postsynaptic APs. **A**, Representative example showing effects of pre-post pairing of uEPSP and postsynaptic firing of three APs (100 Hz, post) with $\Delta t = 10$ ms. Test EPSPs were evoked by electrical stimulation. Pairing involved uncaging of glutamate to produce a uEPSP <5.0 mV in amplitude. **B**, Group average ($n = 6$) in which each point is the average of three consecutive EPSPs (1 min).

gic pathway and to approximate the conditions achieved by glutamate uncaging.

The two-photon imaging demonstrated a significant difference in the calcium levels evoked by pre-post stimulation compared with post-pre stimulation when three action potentials were evoked. To investigate the effects on plasticity, we tested the effect of pairing an EPSP with a subsequent action potential burst (three APs occurring at 100 Hz, $\Delta t = 10$ ms, 60 pairings). This resulted in the induction of t-LTD ($-35.5 \pm 4.2\%$, $n = 13$, $p < 0.01$, paired t test; Fig. 4A). Changes in the EPSP amplitude were not associated with any changes in input resistance or resting membrane potential. In contrast to the pre-post pairing protocol, pairing in the post-pre condition ($\Delta t = -30$ ms relative to first spike) caused no t-LTD ($-1.9 \pm 8.6\%$, $n = 10$, not significant; Fig. 4B).

To test whether the STDP effects were due to the action potentials or EPSPs alone (independent of pairing), we tested the effects of a single EPSP without action potentials, or three action potentials without an EPSP, evoked as in the STDP protocols. In these cases, the EPSP amplitude was not significantly changed by presynaptic simulation alone ($-11.6 \pm 8.3\%$, $n = 6$; Fig. 5A) or by bursts of three action potentials alone ($-11.3 \pm 6.8\%$, $n = 9$; Fig. 5B). In contrast to the effects of burst of three action potentials in the STDP protocols, when single action potentials were used, no long-term changes were observed using either pre-post protocols ($-6.4 \pm 17.4\%$, $n = 6$; Fig. 5C) or post-pre protocols ($-11.2 \pm 7.0\%$, $n = 4$; Fig. 5D).

Combining the $[Ca^{2+}]_i$ measures with t-LTD measures, as in Figure 6, suggests that a critical factor in t-LTD induction is the ability of the stimulation protocol to produce a supralinear increase in $[Ca^{2+}]_i$. As shown in Figure 6A, pairing protocols involving a single action potential did not lead to significant change in EPSPs. When pairing protocols involving three action potentials were tested, the only condition that induced t-LTD was pre-post stimulation (Fig. 6B). This was also the condition that produced a supralinear increase in $[Ca^{2+}]_i$ that resulted in levels
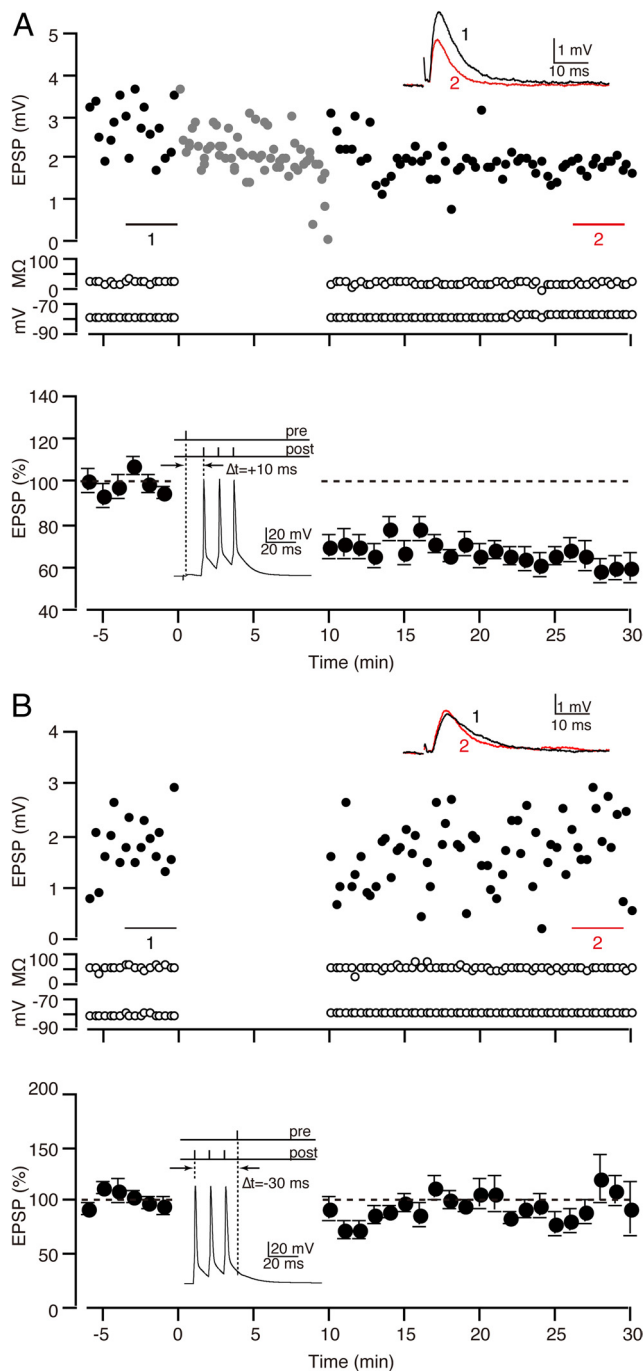
Figure 4. Spike-timing-dependent t-LTD in the striatum. *A*, Pre-post pairing induced t-LTD in the striatum. Top, Representative example of changes in EPSP amplitude induced by pairing electrically evoked EPSPs with postsynaptic firing of three APs (100 Hz, post) with $\Delta t = 10$ ms. Pairing was repeated 60 times at 0.1 Hz. Inset, Superimposed traces of an average of consecutive evoked EPSPs (average of 12 traces at indicated time points) before and after pairing protocols. Gray circles, EPSP amplitudes during pairing protocol. Membrane resistance and membrane potentials were monitored over the course of the experiment. Bottom, Group average ($n = 13$) in which each point is the average of three consecutive EPSPs (1 min). *B*, Post-pre pairing [electrically evoked EPSPs with postsynaptic firing of three APs (100 Hz, post) with $\Delta t = -30$ ms] induced no changes. Pairing was repeated 60 times at 0.1 Hz. Responses during pairing not shown due to preceding spikes. Same conventions as in *A*. Top, Representative example. Bottom, Group average ($n = 10$).

that were significantly greater $[Ca^{2+}]_i$ than any other condition (Fig. 6*C,D*). These findings suggest t-LTD is more affected by spine $[Ca^{2+}]_i$ and less by pairing sequence or number of spikes, since t-LTD is only seen when the change in spine $[Ca^{2+}]_i$ ex-

ceeds 1 μM, corresponding to conditions under which a supralinear increase in spine $[Ca^{2+}]_i$ occurred.

Intracellular calcium is necessary for pre-post spike-time-dependent LTD
To test whether there is a causal relationship between supralinear Ca^{2+} increases and t-LTD, the t-LTD induced by pre-post protocols was investigated using recording pipettes containing Ca^{2+} buffers, EGTA or BAPTA, to buffer intracellular calcium of postsynaptic cells. Loading cells with these buffers at 5 mM significantly blocked pre-post t-LTD ($-7.6 \pm 10.6\%$, two samples of EGTA and four BAPTA; Fig. 7*B*), showing that a rise in intracellular calcium is necessary for striatal spike-time-dependent t-LTD.

Kerr and Plenz (2002, 2004) and Carter and Sabatini (2004) showed that under depolarizing conditions Ca^{2+} influx through the NMDA-type glutamate receptors (NMDARs) results in supralinear boosting of the Ca^{2+} signal. To investigate whether such boosting underlies the effects of timing conditions on t-LTD induction, we examined the effects blocking NMDARs on t-LTD. Contrary to expectations, the NMDAR blocker D-APV (50 μM) failed to block t-LTD induced by our pre-post pairing protocols ($-31.0 \pm 8.8\%$, $n = 12$; Fig. 7*A*). The independence of t-LTD from NMDAR activity in the context of the calcium dependence suggests that boosting of Ca^{2+} influx through the NMDAR-associated channels is not the basis of t-LTD induction, though it does not exclude such a mechanism from being involved in other protocols. However, the calcium chelators BAPTA and EGTA blocked the induction of t-LTD, consistent with a causal role of intracellular Ca^{2+} in t-LTD.

Another possible source of Ca^{2+} influx is through voltage-sensitive calcium channels (Cherubini and Lanfumey, 1987). To investigate the possible involvement of voltage-sensitive calcium channels in t-LTD, we tested the effect of nimodipine on t-LTD induction (Fig. 7*C*). Nimodipine (10 μM) blocked t-LTD ($-8.0 \pm 4.2\%$, $n = 7$); however, a lower dose of nimodipine (1 μM) was not effective in blocking t-LTD ($-23.0 \pm 5.9\%$, $n = 5$). Different populations of VSCCs are expressed on striatal neurons. The dose-dependent effect indicates that the channels mediating the Ca^{2+} influx necessary for t-LTD induced by the pre-post protocol described in this paper are VSCCs of the $Ca_V1.3\ \alpha_1$ type, because they are blocked by 10 μM nimodipine, but only partially blocked by 1 μM nimodipine (IC$_{50} = 2.7\ \mu$M) (Xu and Lipscombe, 2001).

When these doses were tested for their effect on spine $[Ca^{2+}]_i$ transients evoked by pre-post protocols, we found that, as in t-LTD, nimodipine 10 μM reduced the spine $[Ca^{2+}]_i$ transient significantly ($0.76 \pm 0.19\ \mu$M, $n = 5$, compared with control values $1.38 \pm 0.15\ \mu$M, $n = 11$, $p < 0.05$), but nimodipine 1 μM had no significant effect ($1.10 \pm 0.17\ \mu$M, $n = 5$). Nimodipine 10 μM also abolished the supralinear component of the increase in spine $[Ca^{2+}]_i$ (as measured by the ratio of pre-post stimulation to the sum of prestimulation and poststimulation given individually). Under control conditions, compared with the algebraic sum of the uEPSP and action potential responses, pre-post pairing produced a greater ($150.5 \pm 11.1\%$, $n = 11$) increase in spine $[Ca^{2+}]_i$. Similarly, in the presence of nimodipine (1 μM) pre-post pairing also produced a greater increase ($143.2 \pm 17.2\%$, $n = 5$). However, in the presence of the higher dose of nimodipine (10 μM), the supralinear component was reduced and not significantly different from the linear sum ($110.2 \pm 5.7\%$, $n = 5$). These data show that the $Ca_V1.3\ \alpha_1$-type channels blocked by 10 μM

nimodipine are necessary for the supra-linear component of the Ca^{2+} transient as well as t-LTD induction.

Discussion

Intracellular Ca^{2+} signaling plays a key role in the regulation of synaptic plasticity in many brain systems. We report here that activity-dependent changes in cytosolic $[Ca^{2+}]$ in the dendritic spines of projection neurons of the neostriatum are sensitive to the relative timing of neurotransmitter release and postsynaptic spikes. Ca^{2+} signals in the spine are increased by either uncaging of glutamate or by induction of postsynaptic spikes. When these are combined, the resulting Ca^{2+} signal is greater than the sum of the individual contributions, but only if glutamate uncaging precedes postsynaptic spikes by 10 ms. This supralinear increase does not occur when the timing sequence is reversed, in which case the Ca^{2+} signal is as predicted by the sum of the individual contributions. In parallel experiments, we also measured plasticity of the corticostriatal synapses induced by the same temporal sequences using EPSPs evoked by electrical stimulation. We found that the pre-post timing protocols that caused supralinear Ca^{2+} increases caused t-LTD, in contrast to post-pre timing, which induced no significant changes in synaptic efficacy. A causal relationship between elevated cytosolic Ca^{2+} concentration and t-LTD was confirmed by blockade of t-LTD by intracellular Ca^{2+} chelators and a Ca^{2+} channel antagonist. Together, these results show for the first time that the spike-time-dependent induction of t-LTD in the mouse corticostriatal pathway is triggered by a dendritic spine cytosolic Ca^{2+} signal, which becomes suprathreshold under conditions of pre-post spike timing, and is mediated by $Ca_V1.3\ \alpha_1$-type VSCCs.

Investigations in many different systems have shown, similarly, that cytosolic Ca^{2+} changes can signal the occurrence of various types of coincidence of presynaptic and postsynaptic activity (Larkum et al., 1999; Bender et al., 2006; Nevian and Sakmann, 2006). In the striatum, Kerr and Plenz (2002, 2004) measured dendritic Ca^{2+} using fluorimetry and found that increases were maximal for action potentials occurring 10–20 ms after a barrage of presynaptic activity, and greater than the sum of the changes evoked by the action potentials or presynaptic barrages alone. Similarly, Carter and Sabatini (2004) found that when neurons were depolarized to -50 mV, the Ca^{2+} influx associated with action potentials evoked 20 ms after a uEPSP was greater than would be expected from summation of the calcium influx associated with action potentials and uEPSPs occurring independently. The present study extends these findings by showing that timing-dependent boosting of the calcium influx occurs when a short burst of three action potentials is evoked 10 ms after a uEPSP, even if cells are initially at resting membrane potential and not further depolarized by a presynaptic barrage or depolarization to -50 mV. This boosting is only seen in the spine head and not in the adjacent dendrite, consistent with the chemical compartmentalization of Ca^{2+} in dendritic spines (Wickens, 1988). Boosting did not occur with reversed timing, nor when only one action potential was evoked. The latter finding is in contrast to the situation in cortical neurons where several studies
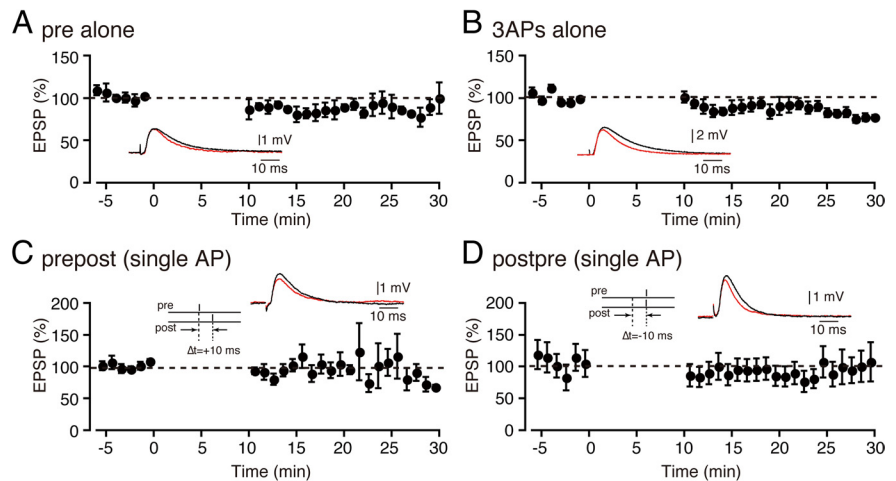
Figure 5. Failure to induce t-LTD using unpaired stimuli or single action potentials. **A**, Unpaired presynaptic stimulation (EPSP alone, repeated at 0.1 Hz) does not induce t-LTD ($n = 6$). **B**, Unpaired postsynaptic stimulation (three action potentials at 100 Hz, repeated at 0.1 Hz) does not induce t-LTD ($n = 9$). **C**, Pre-post protocol fails to induce t-LTD if postsynaptic activity is a single action potential ($n = 6$). **D**, Post-pre protocol induces no change ($n = 4$). Insets, Superimposed traces of an average of consecutive EPSPs (12 traces) before (black) and 14 min after (red) pairing-protocols. Same conventions as in Figure 3.
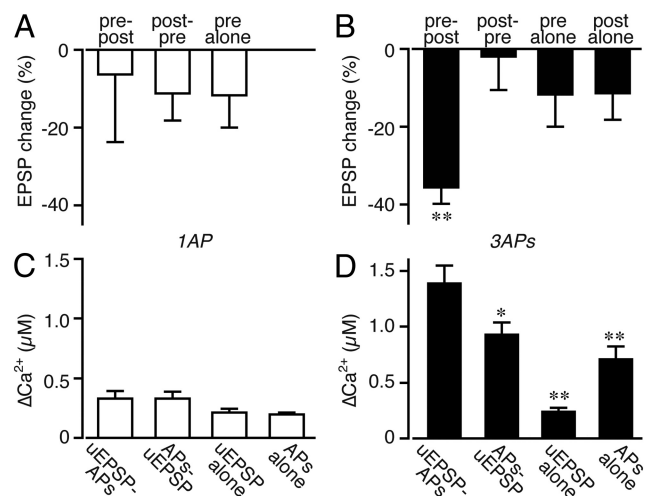
Figure 6. A spine $[Ca^{2+}]_i$ threshold for t-LTD. **A**, Plasticity (EPSP changes) produced by pairing an EPSP and a single AP at $\Delta t = 10$ ms (pre-post), a single AP and an EPSP at $\Delta t = -10$ ms (post-pre), and an EPSP alone (pre alone). **B**, Plasticity (EPSP changes) caused by pairing an EPSP and three APs at $\Delta t = 10$ ms (pre-post), three APs and an EPSP at $\Delta t = -30$ ms (post-pre), an EPSP alone (pre alone) and three APs (post alone). **C, D**, Changes in spine $[Ca^{2+}]_i$ evoked by the pairing protocols in **A** ($n = 4$) and **B** ($n = 11$). *$p < 0.05$, **$p < 0.01$.

have shown that the pairing of a single AP with an EPSP is sufficient to induce t-LTD, while pairing with bursts of APs is sufficient to induce LTP (Magee and Johnston, 1997; Nevian and Sakmann, 2006; Wittenberg and Wang, 2006), and possibly reflects differences in the molecular cascades expressed in the spiny projections neurons.

We found that blocking NMDA receptors did not block pre-post t-LTD. This result is consistent with findings using conventional HFS induction protocols (Calabresi et al., 1992; Walsh, 1993). Calabresi et al. (1999) also found that brief focal application of glutamate induced LTD. Since chemical and HFS-induced LTD were occlusive, this suggests a common mechanism, which is also probable using glutamate uncaging as in the present experiments. The lack of effect of NMDA blockade seems surprising at first, in light of previous studies showing that the boosting of
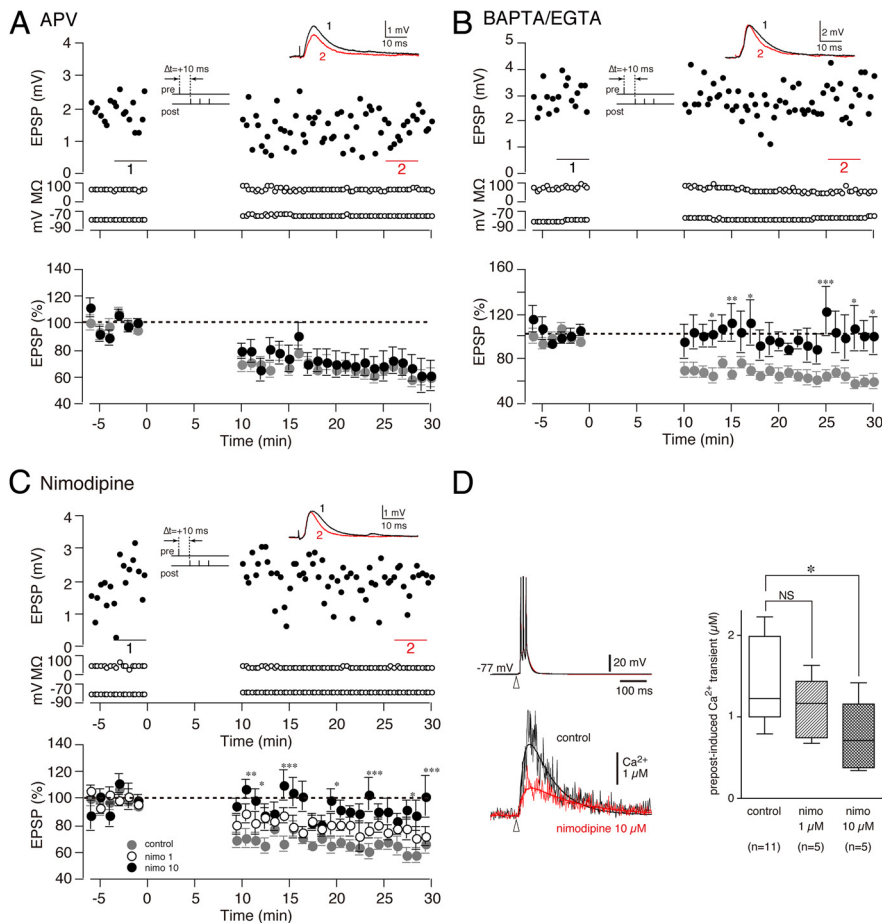
Figure 7. Postsynaptic $[Ca^{2+}]_i$ increase is necessary for pre-post t-LTD. **A**, Activation of the NMDA receptor is not necessary for the induction of the pre-post t-LTD. Bath application of the NMDA blocker D-APV (50 μM) did not block pre-post t-LTD ($n = 12$, filled circles). **B**, Intracellular Ca^{2+} chelators blocked pre-post t-LTD. Top, Representative example of showing that postsynaptic inclusion of a Ca^{2+} chelator, BAPTA (5 mM), significantly blocks pre-post t-LTD. Bottom, Group average of effects of postsynaptic Ca^{2+} chelators (average of cells loaded with BAPTA, $n = 4$ or EGTA, $n = 2$; filled circles). **C**, Nimodipine 10 μM significantly blocked pre-post t-LTD ($n = 7$; filled circles) but nimodipine 1 μM did not block pre-post t-LTD ($n = 5$; open circles). **D**, Effect of nimodipine on pre-post induced Ca^{2+} transients. Left, Upper trace, voltage trace from recorded cell; lower trace, comparison of Ca^{2+} transient under control conditions and in the presence of nimodipine 10 μM. Right, Group average data show significant effect of nimodipine 10 μM on pre-post induced Ca^{2+} transients. *$p < 0.05$, **$p < 0.01$, ***$p < 0.001$.

$[Ca^{2+}]_i$ by pre-post protocols was due to enhanced Ca^{2+} influx through NMDA receptor-associated channels (Carter and Sabatini, 2004; Kerr and Plenz, 2004). However, the boosting reported by Carter and Sabatini (2004) was only seen when neurons were depolarized by current injection, in contrast to the present experiments in which the neurons were at resting potential before spikes were evoked. Similarly, the boosting reported by Kerr and Plenz (2004), which also required voltage-sensitive opening of NMDA receptor-associated channels, was elicited by a barrage of presynaptic activity rather than a single EPSP as in the present experiments. The pre-post protocol used in the current experiments is unlikely to cause NMDA receptor-associated channel mediated boosting, consistent with our finding that t-LTD was not blocked by NMDA antagonists.

Previous work using two-photon laser scanning microscopy has shown that somatic spikes can cause opening of VSCCs in proximal dendrites and spines of spiny projection neurons of the striatum (Carter and Sabatini, 2004). This work has shown that multiple VSCC classes contribute to Ca^{2+} signals in MSN dendrites and spines. Different classes of VSCC are activated depending on resting membrane potential. Depolarization from resting

potentials activates L- and R- type channels. In the present study, t-LTD induction was blocked by 10 μM nimodipine but not 1 μM nimodipine. At 10 μM, nimodipine blocks $Ca_V 1.3$ α_1 channels, which have an IC_{50} of 2.7 μM (Xu and Lipscombe, 2001). This does not completely abolish spine $[Ca^{2+}]_i$ transients, but rather selectively blocks the supralinear increase in spine $[Ca^{2+}]_i$ that is necessary for t-LTD and requires pre-post timing. Previous studies have shown that nimodipine decreases the spine $[Ca^{2+}]_i$ influx brought about by depolarization (Higley and Sabatini, 2010). The present results extend these findings by showing that the supralinear component of the spine $[Ca^{2+}]_i$ transient mediated by $Ca_V 1.3$ α_1 channels is necessary for t-LTD. This does not exclude activation of other mechanisms, such as NMDA-associated channels, under the more depolarized conditions used in other STDP studies.

A number of laboratories have reported results of striatal STDP that appear to differ from the present results. Fino et al. (2005) found that pre-post stimulation caused t-LTD, but post-pre timing caused LTP. In contrast to both Fino et al. (2005) and the present study, Pawlak and Kerr (2008) reported t-LTP with pre-post timing. However, they applied 50 μM picrotoxin (GABA$_A$ receptor blocker) and 10 μM glycine (NMDA receptor coagonist). Fino et al. (2010) also reported t-LTP under conditions of blockade of GABAergic transmission. In light of our previous studies showing that dopamine reverses the LTD that normally follows HFS (Wickens et al., 1996) and that LTP under NMDA-facilitated conditions is blocked by dopamine antagonists (Kerr and Wick-

ens, 2001), we suggest that coincident release of dopamine may explain the t-LTP reported by Pawlak and Kerr (2008) and Fino et al. (2010) under of blockade of GABAergic transmission. In support of this, electrical stimulation of the cortex causes release of dopamine in the striatum, and this is increased by GABA antagonists (Juranyi et al., 2003). Furthermore, the t-LTP was prevented by blocking dopamine receptors (Pawlak and Kerr, 2008), indicating a causal role of dopamine in t-LTP. In the present experiments, the ACSF did not contain glycine or picrotoxin, and the stimulation was deliberately chosen to be of low intensity to avoid activating dopamine release, so that we could isolate t-LTD and elucidate underlying mechanisms.

In a study using a somewhat different stimulation protocol in which a theta-burst pattern was applied within the striatal neuropil, Shen et al. (2008) measured plasticity in identified striatal neurons. Notably, in neurons that expressed the dopamine D1 receptors, pre-post stimulation also led to t-LTD, but only under dopamine-depleted conditions. The present results are very similar to those obtained by Shen et al. (2008) under dopamine-depleted conditions, consistent with the low intensity of cortical stimulation used in the present experiments, which avoids acti-

vating the dopaminergic fibers in the slice because they have a higher rheobase.

In summary, the present study has provided evidence that t-LTD is induced by conditions that give rise to supralinear increases in calcium concentration in dendritic spines, but in the absence of phasic dopamine release. These increases are seen in the dendritic spines but not in the underlying dendritic shaft, suggesting a spine locus of control for this form of t-LTD. The supralinearity necessary for t-LTD induction depends on L-type calcium channels. Finally, we note that pre-post timing may have a functional significance in learning, because such timing relations are consistent with a causal influence of presynaptic activity on postsynaptic cell firing, which may be important in eligibility for synaptic modification during learning (Izhikevich, 2007). Further work should investigate possible modulation of this form of synaptic plasticity by dopamine, as predicted by the effects of dopamine on LTD induced by HFS protocols.

References

Adermark L, Lovinger DM (2007) Combined activation of L-type Ca2+ channels and synaptic transmission is sufficient to induce striatal long-term depression. J Neurosci 27:6781–6787.

Bauswein E, Fromm C, Preuss A (1989) Corticostriatal cells in comparison with pyramidal tract neurons: contrasting properties in the behaving monkey. Brain Res 493:198–203.

Bender VA, Bender KJ, Brasier DJ, Feldman DE (2006) Two coincidence detectors for spike timing-dependent plasticity in somatosensory cortex. J Neurosci 26:4166–4177.

Bonsi P, Pisani A, Bernardi G, Calabresi P (2003) Stimulus frequency, calcium levels and striatal synaptic plasticity. Neuroreport 14:419–422.

Calabresi P, Maj R, Pisani A, Mercuri NB, Bernardi G (1992) Long-term synaptic depression in the striatum: physiological and pharmacological characterization. J Neurosci 12:4224–4233.

Calabresi P, Pisani A, Mercuri NB, Bernardi G (1994) Post-receptor mechanisms underlying striatal long-term depression. J Neurosci 14:4871–4881.

Calabresi P, Pisani A, Mercuri NB, Bernardi G (1996) The corticostriatal projection: from synaptic plasticity to dysfunctions of the basal ganglia. Trends Neurosci 19:19–24.

Calabresi P, Centonze D, Gubellini P, Marfia GA, Bernardi G (1999) Glutamate-triggered events inducing corticostriatal long-term depression. J Neurosci 19:6102–6110.

Calabresi P, Picconi B, Tozzi A, Di Filippo M (2007) Dopamine-mediated regulation of corticostriatal synaptic plasticity. Trends Neurosci 30:211–219.

Carter AG, Sabatini BL (2004) State-dependent calcium signaling in dendritic spines of striatal medium spiny neurons. Neuron 44:483–493.

Cherubini E, Lanfumey L (1987) An inward calcium current underlying regenerative calcium potentials in rat striatal neurons in vitro enhanced by BAY K 8644. Neuroscience 21:997–1005.

Day M, Wang Z, Ding J, An X, Ingham CA, Shering AF, Wokosin D, Ilijic E, Sun Z, Sampson AR, Mugnaini E, Deutch AY, Sesack SR, Arbuthnott GW, Surmeier DJ (2006) Selective elimination of glutamatergic synapses on striatopallidal neurons in Parkinson disease models. Nat Neurosci 9:251–259.

Fino E, Glowinski J, Venance L (2005) Bidirectional activity-dependent plasticity at corticostriatal synapses. J Neurosci 25:11279–11287.

Fino E, Paille V, Cui Y, Morera-Herreras T, Deniau JM, Venance L (2010) Distinct coincidence detectors govern the corticostriatal spike timing-dependent plasticity. J Physiol 588:3045–3062.

Herrling PL, Morris R, Salt TE (1983) Effects of excitatory amino acids and their antagonists on membrane and action potentials of cat caudate neurones. J Physiol 339:207–222.

Higley MJ, Sabatini BL (2008) Calcium signaling in dendrites and spines: practical and functional considerations. Neuron 59:902–913.

Higley MJ, Sabatini BL (2010) Competitive regulation of synaptic Ca2+

influx by D2 dopamine and A2A adenosine receptors. Nat Neurosci 13:958–966.

Izhikevich EM (2007) Solving the distal reward problem through linkage of STDP and dopamine signaling. Cereb Cortex 17:2443–2452.

Juranyi Z, Zigmond MJ, Harsing LG Jr (2003) [3H]Dopamine release in striatum in response to cortical stimulation in a corticostriatal slice preparation. J Neurosci Methods 126:57–67.

Kawaguchi Y, Wilson CJ, Emson PC (1989) Intracellular recording of identified neostriatal patch and matrix spiny cells in a slice preparation preserving cortical inputs. J Neurophysiol 62:1052–1068.

Kerr JN, Plenz D (2002) Dendritic calcium encodes striatal neuron output during up-states. J Neurosci 22:1499–1512.

Kerr JN, Plenz D (2004) Action potential timing determines dendritic calcium during striatal up-states. J Neurosci 24:877–885.

Kerr JN, Wickens JR (2001) Dopamine D-1/D-5 receptor activation is required for long-term potentiation in the rat neostriatum in vitro. J Neurophysiol 85:117–124.

Kita H (1996) Glutamatergic and GABAergic postsynaptic responses of striatal spiny neurons to intrastriatal and cortical stimulation recorded in slice preparations. Neuroscience 70:925–940.

Larkum ME, Zhu JJ, Sakmann B (1999) A new cellular mechanism for coupling inputs arriving at different cortical layers. Nature 398:338–341.

Magee JC, Johnston D (1997) A synaptically controlled, associative signal for Hebbian plasticity in hippocampal neurons. Science 275:209–213.

Nevian T, Sakmann B (2006) Spine Ca2+ signaling in spike-timing-dependent plasticity. J Neurosci 26:11001–11013.

Noguchi J, Matsuzaki M, Ellis-Davies GC, Kasai H (2005) Spine-neck geometry determines NMDA receptor-dependent Ca2+ signaling in dendrites. Neuron 46:609–622.

Packard MG, Knowlton BJ (2002) Learning and memory functions of the basal ganglia. Annu Rev Neurosci 25:563–593.

Pawlak V, Kerr JN (2008) Dopamine receptor activation is required for corticostriatal spike-timing-dependent plasticity. J Neurosci 28:2435–2446.

Shen W, Flajolet M, Greengard P, Surmeier DJ (2008) Dichotomous dopaminergic control of striatal synaptic plasticity. Science 321:848–851.

Shindou T, Arbuthnott GW, Wickens JR (2008) Actions of adenosine A2A receptors on synaptic connections of spiny projection neurons in the neostriatal inhibitory network. J Neurophysiol 99:1884–1889.

Surmeier DJ, Ding J, Day M, Wang Z, Shen W (2007) D1 and D2 dopamine-receptor modulation of striatal glutamatergic signaling in striatal medium spiny neurons. Trends Neurosci 30:228–235.

Turner RS, DeLong MR (2000) Corticostriatal activity in primary motor cortex of the macaque. J Neurosci 20:7096–7108.

Walsh JP (1993) Depression of excitatory synaptic input in rat striatal neurons. Brain Res 608:123–128.

Wickens JR (1988) Electrically coupled but chemically isolated synapses: dendritic spines and calcium in a rule for synaptic modification. Prog Neurobiol 31:507–528.

Wickens JR (2009) Synaptic plasticity in the basal ganglia. Behav Brain Res 199:119–128.

Wickens JR, Begg AJ, Arbuthnott GW (1996) Dopamine reverses the depression of rat cortico-striatal synapses which normally follows high frequency stimulation of cortex in vitro. Neuroscience 70:1–5.

Wilson CJ (1986) Postsynaptic potentials evoked in spiny neostriatal projection neurons by stimulation of ipsilateral and contralateral neocortex. Brain Res 367:201–213.

Wilson CJ, Groves PM (1980) Fine structure and synaptic connection of the common spiny neuron of the rat neostriatum: a study employing intracellular injection of horseradish peroxidase. J Comp Neurol 194:599–615.

Wittenberg GM, Wang SS (2006) Malleability of spike-timing-dependent plasticity at the CA3-CA1 synapse. J Neurosci 26:6610–6617.

Xu W, Lipscombe D (2001) Neuronal Ca(V)1.3alpha(1) L-type channels activate at relatively hyperpolarized membrane potentials and are incompletely inhibited by dihydropyridines. J Neurosci 21:5944–5951.

Yasuda R, Nimchinsky EA, Scheuss V, Pologruto TA, Oertner TG, Sabatini BL, Svoboda K (2004) Imaging calcium concentration dynamics in small neuronal compartments. Sci STKE 2004:pl5.

Yin HH, Knowlton BJ (2006) The role of the basal ganglia in habit formation. Nat Rev Neurosci 7:464–476.